



# Synthesis of carbon/SiO<sub>2</sub> core-sheath nanofibers with Co-Fe nanoparticles embedded in via electrospinning for high-performance microwave absorption

Ziyu Zhang<sup>1,2</sup> · Yehao Zhao<sup>1,2</sup> · Zihao Li<sup>1,2</sup> · Lujie Zhang<sup>1,2</sup> · Zixuan Liu<sup>1,2</sup> · Zhenkun Long<sup>1,2</sup> · Yunjia Li<sup>1,2</sup> · Yao Liu<sup>1,2</sup> · Runhua Fan<sup>2,3</sup> · Kai Sun<sup>3</sup> · Zidong Zhang<sup>1,2</sup>

Received: 3 August 2021 / Revised: 9 September 2021 / Accepted: 16 September 2021 / Published online: 8 October 2021  
© The Author(s), under exclusive licence to Springer Nature Switzerland AG 2021

## Abstract

As an excellent microwave absorption material, the in-depth study of carbon-based nanofibers' absorbing mechanism is of great significance for subsequent applications. In this paper, carbon/SiO<sub>2</sub> core-sheath nanofibers with Co-Fe nanoparticles embedded in were synthesized by electrospinning and carbonization. The morphology, microstructure, magnetic properties, and microwave absorption performance of the composite nanofibers were characterized in detail. The results show that the maximum reflection loss (RL) could reach to -59.6 dB, and the maximum effective absorption bandwidth (RL < -10 dB) achieved 4.6 GHz with only 1.43 mm thickness. It is indicated that the introduction of SiO<sub>2</sub> improved the impedance matching, and formed a large number of heterogeneous interfaces with carbon nanofibers and Co-Fe nanoparticles, resulting in the interfacial polarization. Co-Fe nanoparticles could enhance the magnetic loss by small size effect, while the graphite lattice was damaged to a certain extent, causing the dipole polarization. This work provides an effective idea for the synthesis and performance optimization of high-performance microwave absorption materials.

**Keywords** Co-Fe@C/SiO<sub>2</sub> nanofibers · Electrospinning · Wave-absorbing mechanism · Core-sheath structure

## 1 Introduction

In recent years, with the development and maturity of electromagnetic (EM) wave technology, the popularity of wireless communication has not only brought great convenience to people, but also brought serious problems such as EM radiation and EM interference, resulting in the control failure of electronic equipment and poor communication quality. Moreover, some studies even indicate that EM radiation even poses a potential threat to human life and health [1–6]. In the military field, the burgeon of radar technology also puts

forward higher requirements for stealth technology used in military equipment such as fighter jets and destroyer [7–10]. In order to solve the above problems, it is urgent to develop a material with efficient microwave absorption properties.

The key point to obtain this high-performance microwave absorption material is to achieve both the impedance matching and ample EM attenuation capability. Generally speaking, the design of microwave absorption materials mainly includes these two aspects. Among them, impedance matching is to make the incident EM wave illuminate in the material smoothly without being reflected out [11, 12], and EM attenuation is to convert the incident EM wave energy into thermal energy [13, 14], so as to achieve the purpose of absorbing EM wave. The specific expressions of these two characteristics are calculated by permittivity and permeability, so the EM parameters of the material itself become an especially important standard for material selection.

Up to now, there are many kinds of materials used in microwave absorption, such as ferrites, magnetic metals, and carbon materials. For ferrites and magnetic metals, high density and unstable high temperature performance limit their application [15, 16]. Carbon materials represented by

✉ Zidong Zhang  
zhangzidong@sdu.edu.cn

<sup>1</sup> School of Materials Science and Engineering, Shandong University, Jinan 250061, China

<sup>2</sup> Key Laboratory for Liquid–Solid Structural Evolution and Processing of Materials (Ministry of Education), Shandong University, Jinan 250061, China

<sup>3</sup> College of Ocean Science and Engineering, Shanghai Maritime University, Shanghai 201306, China

graphene, carbon nanotubes, and carbon nanofibers have been widely used in the preparation of EM wave absorption materials because of their excellent conductivity, large specific surface area, low density, low cost, and stable physicochemical properties [17–23]. As a one-dimensional structural material, carbon nanofibers can form a conductive network, while the larger length-diameter ratio promotes the conduction of electrons and greatly increases the conductivity loss of the material. However, simple carbon materials will cause impedance mismatching because of their high conductivity, resulting in a considerable number of incident EM waves being reflected on the surface of the material, which cannot give full play to its excellent EM attenuation characteristics. Therefore, it is a method widely used by researchers to composite carbon materials with other materials and optimize the microwave absorbing properties of materials through the structure and coordination of multi-components. For instance, Zhang et al. prepared Fe@Fe<sub>3</sub>O<sub>4</sub>-C nanocomposites, whose special core-shell structure effectively improves the dielectric loss and magnetic loss, the maximum RL can reach -48.36 dB, with the maximum effective absorption bandwidth up to 7.9 GHz at a thickness of 2.27 mm [24]. Lv et al. pyrolyzed Co-based metal organic framework into composite materials containing Co magnetic nanoparticles embedded in porous carbon matrix. The maximum RL reached -35.3 dB, and the effective absorption bandwidth was 5.8 GHz corresponding to a thickness of 2.5 mm. It was found that the porous structure and the synergistic effect of multi-components significantly enhanced the EM wave absorption [25].

Although great breakthroughs have been made in the research progress, it is still a problem to find more suitable material for high performance. Co-Fe nanoparticles not only have the loss characteristics of traditional magnetic EM wave absorption materials, but their small size effect and surface effect can also further improve the wave-absorbing properties of magnetic EM wave absorption materials [26], so they are a type of wave-absorbing materials with great application value and development prospect. Despite that the absorbing properties of carbon materials compounded with ferrites or magnetic metals can be substantially improved, the introduction of these magnetic materials also leads to the increase of conductivity which results in impedance mismatch, so it is necessary to choose a material to balance its permittivity. SiO<sub>2</sub> is a kind of easily available dielectric with low permittivity. When it exists alone, it can only be used as a wave-transparent material, but when compounded with carbon material, its permittivity can be adjusted. When the content of SiO<sub>2</sub> is opportune, impedance matching can be improved obviously, and it also brings more interfaces, enhancing interfacial polarization.

In this work, carbon nanofibers, carbon nanofibers embedded in Co-Fe nanoparticles (Co-Fe@CNFs), and

carbon/SiO<sub>2</sub> core-sheath nanofibers embedded in Co-Fe nanoparticles (Co-Fe@C/SiO<sub>2</sub>NFs) were successfully prepared by electrospinning and carbonization. SiO<sub>2</sub> was uniformly coated on carbon nanofibers, which effectively improved their impedance matching, while the addition of Co-Fe nanoparticles significantly reduced the matching thickness of the materials, so that the material has excellent wave-absorbing properties in the case of thin thickness. The results show that the microwave absorbing properties of carbon nanofibers and carbon nanofibers embedded in Co-Fe nanoparticles are inferior due to impedance mismatch, and the uniform coating of SiO<sub>2</sub> on the basis of Co-Fe@CNFs dramatically improves the impedance matching of the materials, which not only gives sufficient scope to the original attenuation ability of the materials, but also enhances the dipole polarization and interfacial polarization. As a result, high-performance microwave absorption materials have been obtained.

## 2 Experimental

### 2.1 Synthesis of samples

1.0 g polyacrylonitrile (PAN) was added to 8.0 g N,N-dimethylformamide (DMF) and fully dissolved by magnetic stirring at 40 °C. 0.4979 g iron acetylacetonate (IA) and 0.5021 g cobalt acetylacetonate (CA) (the molar ratio of Fe to Co was 1:1) and 1 mL tetraethyl orthosilicate (TEOS) were added to the solution and stirred overnight at 40 °C to form a homogeneous precursor solution. A 20 mL syringe is used to aspirate the precursor solution for electrospinning. The parameters of electrospinning are as follows: the voltage between the lip of the needle and the aluminum foil was 13 kV with the collection distance of 15 cm, and the feeding rate was 0.04 mm/min. Then, the polymer-based precursor fiber was dried in a drying oven at 80 °C for 12 h, and the dried sample was pre-oxidized in a tube furnace at 240 °C for 2 h. After pre-oxidation, the sample was carbonized in nitrogen atmosphere at 750 °C for 2 h to obtain the Co-Fe@C/SiO<sub>2</sub>NFs, denoted as CFCS. The formation of core-sheath structure can be attributed to the phase separation effect [27]. Due to the difference of solubility between TEOS and PAN during the electrospinning process, the volatilization of the surface solvent would promote the formation of a thin layer of solute enrichment on the surface when the fibers were spun out from the nozzle. At the same time, the solute with high solubility in the solution was easier to dissolve, making the insoluble TEOS remain in the outer layer. After carbonization, the fibers with the layer of SiO<sub>2</sub> and the core of carbon were formed. Meanwhile, both Co-Fe/C composite nanofibers without SiO<sub>2</sub> and carbon nanofibers, denoted as CFC and CNFs respectively, were prepared by the same

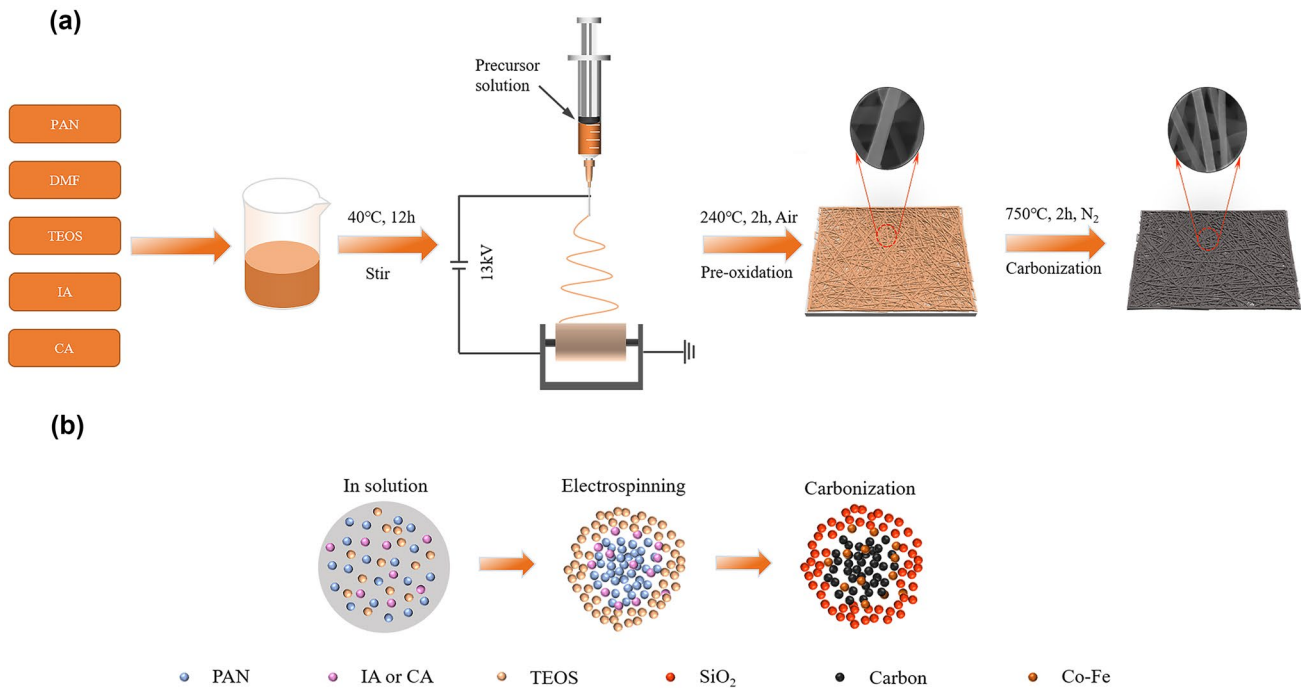


**Fig. 1** Schematic diagram of the fabrication process of CFCS (a) and the formation of core-sheath structure (b)

method as reference group. The specific synthesis process and the formation of the core-sheath structure are shown schematically in Fig. 1.

## 2.2 Characterization

The crystal structure and phase composition of the samples were characterized by X-ray diffraction (XRD, 2500PC) with a Cu K $\alpha$  radiation source. The micro-morphology of the samples was analyzed by field-emission scanning electron microscope (SEM, SU-70) and transmission electron microscope (TEM, JEOL JEM-2100). The graphitization degree of the sample was detected by Raman spectrum (Renishaw in Via). The hysteresis loop of the sample at room temperature was measured by a vibrating sample magnetometer (VSM, Lake Shore, 7404). In order to measure the microwave absorbing properties of the samples, the prepared CNFs, CFC, and CFCS were mixed with paraffin wax at a mass fraction of 30% to form uniform coaxial rings denoted as CNFs30, CFC30, and CFCS30 with a thickness of about 2.5 mm, an outer diameter of 7.0 mm, and an inner diameter of 3.0 mm. The complex permittivity ( $\epsilon_r = \epsilon' - j\epsilon''$ ) and complex permeability ( $\mu_r = \mu' - j\mu''$ ) of the samples were measured in the frequency range of 2–18 GHz by vector network analyzer (Agilent, E5071C). The method for measuring was coaxial transmission/reflection mode, and the calibration was strictly performed before measurement. Then,

the absorbing properties of the materials were expressed by calculation.

## 3 Results and discussion

Figure 2a shows the XRD spectrum of CNFs, CFC, and CFCS. The wide peaks of the three samples around 25° correspond to graphite. The peaks are broadened due to the presence of amorphous carbon. Different from CNFs and CFC, CFCS has two weak peaks around 22° to 25°, and the peak at a smaller angle can be considered to be caused by the low crystallization degree of SiO<sub>2</sub>. The peaks of CFC and CFCS at 44.8°, 65.3°, and 82.7° refer to the (110), (200), (211) crystal plane of Co-Fe 28 (JCPDS No. 49–1567), respectively, which proves that Co-Fe@C/SiO<sub>2</sub>NFs have been successfully prepared.

The SEM images of the three samples are shown in Fig. 3a–c, from which we can see that the fibers of these samples are connected to each other and exhibit a three-dimensional grid structure. At high magnification, the diameter of the fibers can be observed between 150 and 300 nm (Fig. 3d–f). For CNFs, the surface is smooth and homogeneous, while the surfaces of CFC and CFCS are relatively rough, with granular protuberances. It can be inferred that the fine grains uniformly distributed on the fiber are Co-Fe nanoparticles reduced by carbon at high temperature. The microstructure of CFCS is also analyzed by TEM. As

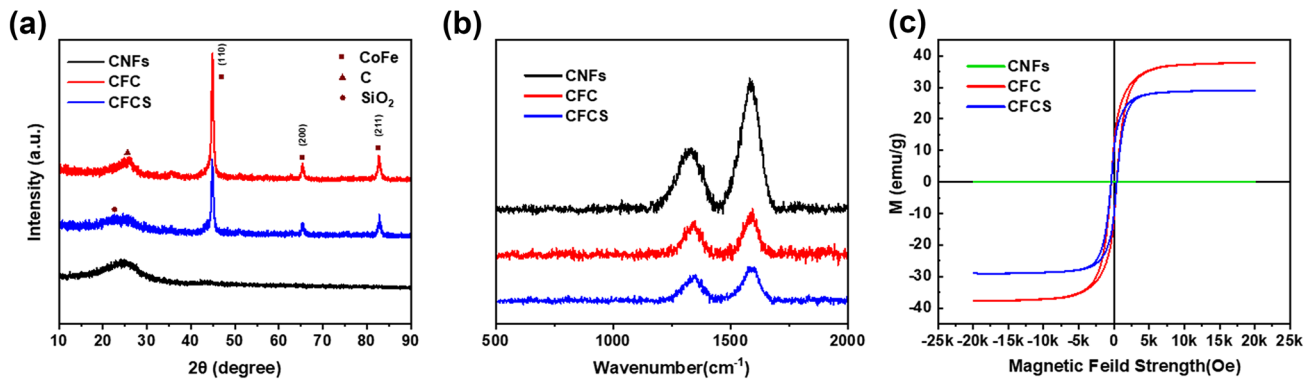


**Fig. 2** XRD patterns (a), Raman spectra (b), and magnetic hysteresis loops (c) of CNFs, CFC, and CFCS

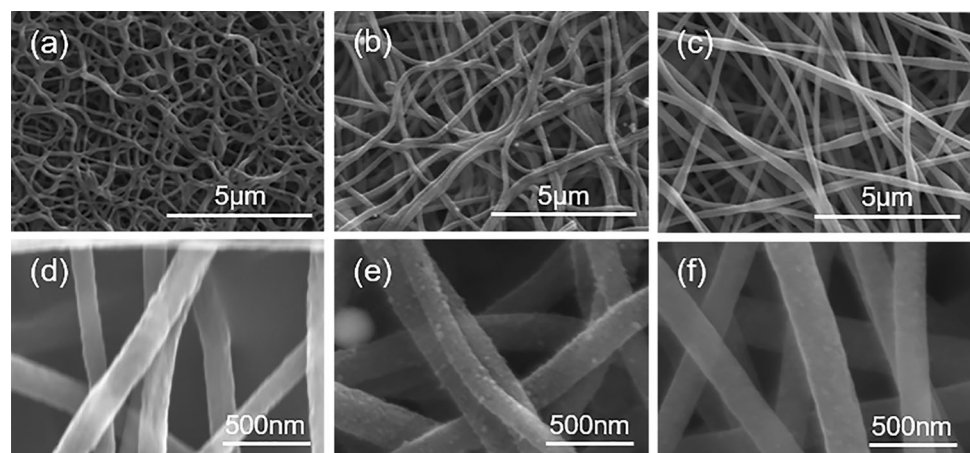
shown in Fig. 4, the size of the particles embedded on the surface of fibers is about 15 nm (Fig. 4a). In Fig. 4b, the crystal plane spacing of the particles is 0.202 nm, which corresponds to the crystal plane of Co-Fe alloy. In addition, the selected-area electron diffraction (SAED) pattern corresponds well to the results of XRD patterns, indicating that the generated Co-Fe nanoparticles have polycrystalline properties (Fig. 4d). For the surface of the particles, it can be found that there is a cover with crystal plane spacing of 0.404 nm (Fig. 4b), which corresponds to the crystal plane of SiO<sub>2</sub>, proving that the surface SiO<sub>2</sub> is coated on carbon nanofibers. This structure can improve the oxidation resistance and corrosion resistance of the materials, and more importantly, it can improve the impedance matching of the materials, which is conducive to the improvement of microwave absorption properties. Figure 4c indicates that the SiO<sub>2</sub> layer also provides generous interface between carbon and Co-Fe nanoparticles, which effectively enhances the interfacial polarization.

The carbon in the sample is divided into amorphous carbon and graphite carbon. Because the carbon atoms in graphite carbon combine with the adjacent three carbon

atoms with a  $\sigma$  bond by  $sp^2$  hybridization, the six carbon atoms form a regular hexagonal ring in the same plane, which extends into a layered structure. Each carbon atom in the same layer has a p orbital containing a 2p electron, forming an extended  $\pi$  bond, and the electrons can move freely in the plane; therefore, graphite carbon has conductivity, and the degree of graphitization of materials has become an important factor to determine the electrical conductivity of materials [28]. For the Raman spectrum measured as shown in Fig. 2b, we can see that there are two obvious broad peaks near  $1340\text{ cm}^{-1}$  and  $1590\text{ cm}^{-1}$ , which represent the D-band of amorphous carbon and the G-band of graphite carbon [29], respectively. The intensity ratio of D-band to G-band ( $I_D/I_G$ ) can be used as a standard to measure the degree of graphitization. The  $I_D/I_G$  values of the three samples are 0.470, 0.741, and 0.751, respectively, which shows that with the introduction of Co-Fe nanoparticles, the graphite lattice in the sample is destroyed greatly, resulting in many defects and amorphous carbon, resulting in the decrease of the value.

Due to the introduction of Co-Fe nanoparticle, the hysteresis loops of three kinds of samples were tested by VSM. As

**Fig. 3** SEM images of CNFs (a, d), CFC (b, e), and CFCS (c, f)



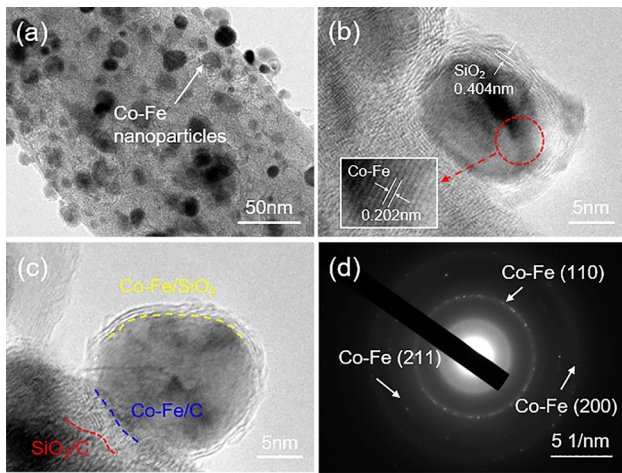


**Fig. 4** TEM and HR-TEM images of CFCS (a–c) and SAED pattern of CFCS (d)

shown in Fig. 2c, CNFs are non-magnetic and their measurement curve is a horizontal straight line. The saturation magnetization ( $M_s$ ) of CFC and CFCS is 37.7 emu/g and 29 emu/g, respectively, and the coercivity ( $H_c$ ) is 400 Oe. Compared with single Co-Fe alloy, it has a higher coercivity, because the size of Co-Fe nanoparticles in the sample is only about 15 nm. It is caused by the increase of surface anisotropy field resulting from its small size effect [26].

In general, the value of RL represents the ability of the material to absorb and lose EM wave, and it is the key standard to evaluate the absorbing performance of the material. It is calculated according to the transmission line theory and the metal backplane model [30, 31]:

$$Z_{in} = Z_0 \sqrt{\epsilon_r / \mu_r} \tanh \left| j(2\pi f d / c) \sqrt{\epsilon_r / \mu_r} \right| \tag{1}$$

$$RL(dB) = 20 \lg \left| \frac{Z_{in} - Z_0}{Z_{in} + Z_0} \right| \tag{2}$$

where  $Z_{in}$  and  $Z_0$  represent the input impedance of the sample and the air,  $f$  is the frequency,  $c$  is the propagation velocity of EM wave in vacuum, and  $d$  is the thickness of the sample.

In order to apply absorber in real life, the RL less than  $-10$  dB is selected as the benchmark for effective absorption of EM waves. For example, Fig. 5 shows the three-dimensional RL of three kinds of samples, which can more intuitively compare the diversity of EM wave absorption between different materials. The maximum RL of CFCS30 is  $-59.6$  dB (Fig. 5a), while that of CFC30 and CNFs30 is only  $-12.7$  dB and  $-10.2$  dB (Fig. 5b and c). Accordingly, CFCS30 has the widest effective absorption bandwidth of 4.6 GHz at 1.43 mm, and that of CFC30 is only 3.1 GHz at 1.09 mm. For CNFs30, there is almost no effective absorption bandwidth. After comparison, it can be concluded that CNFs have the worst wave-absorbing properties without loading anything. After the introduction of Co-Fe nanoparticles, the effective absorbing bandwidth is slightly increased and the matching thickness is also reduced. But it still cannot meet the demand. On the basis of CFC30,  $\text{SiO}_2$  is further added to coat the surface of carbon nanofibers. It is found that although the matching thickness becomes thicker, the absorption intensity and the effective absorption bandwidth are significantly enhanced. Obviously, under the condition that the matching thickness is as thin as possible, these two targets are crucial for the evaluation of wave-absorbing properties.

Table 1 shows the absorption ability of carbon-based absorbers recently reported in the literature. After comparison, it can be found that CFCS30 has thinner thickness and higher absorption strength than other absorbers. Therefore, the results indicate that Co-Fe@C/SiO<sub>2</sub>NFs have the potential to become ultra-thin and efficient wave-absorbing materials.

Then, we explore the reason why the absorbing performance of CFCS30 is so excellent; the EM parameters of three kinds of samples are analyzed. In order to get a well understanding of wave-absorbing mechanism, both

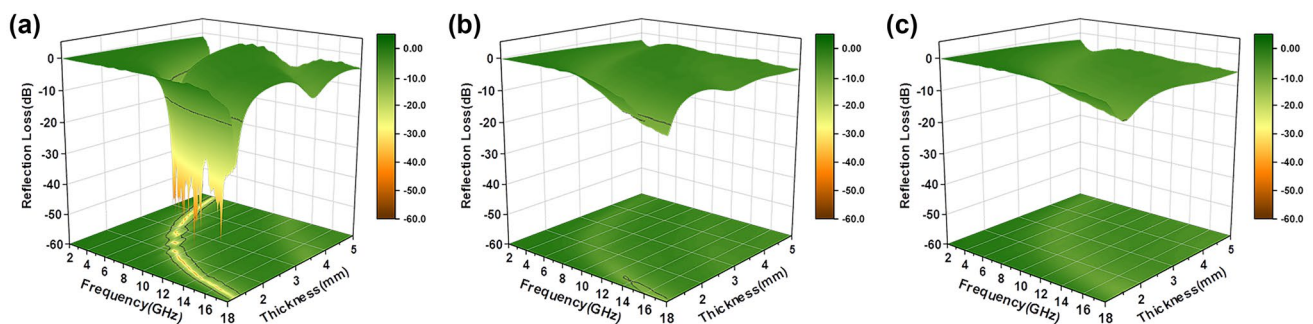


**Fig. 5** 3D reflection loss curves of CFCS30 (a), CFC30 (b), and CNFs30 (c)

**Table 1** Microwave absorption ability of carbon-based absorber in recent reports

Sample	$RL_{\min}$ (dB)	Effective bandwidth (GHz)	Matching thickness (mm)	Ref
N-doped graphene foams	-53.9	4.56	2	Liu et al. [14]
NC@Co/NC carbon nanocages	-52.5	4.4	2.2	Liu et al. [17]
SiC/carbon hybrid nanofibers	-36	4.1	1.5	Huo et al. [19]
Co-C nanofibers	-33.1	4.1	1.5	Shen et al. [32]
Porous hollow Ni/C composites	-55.4	4.4	1.61	Wu et al. [37]
N-doped carbon nanofibers	-48.67	4.9	1.53	Jian et al. [47]
Co-Fe@C/SiO <sub>2</sub> nanofibers	-59.6	4.6	1.43	This work

permittivity and permeability of the three different kinds of samples are investigated by VNA. As well known, the EM parameter is the most important factor affecting the EM

wave absorption characteristics. The real part reflects the energy storage capacity of the material, while the imaginary part reflects the energy loss ability of the material [32]. As

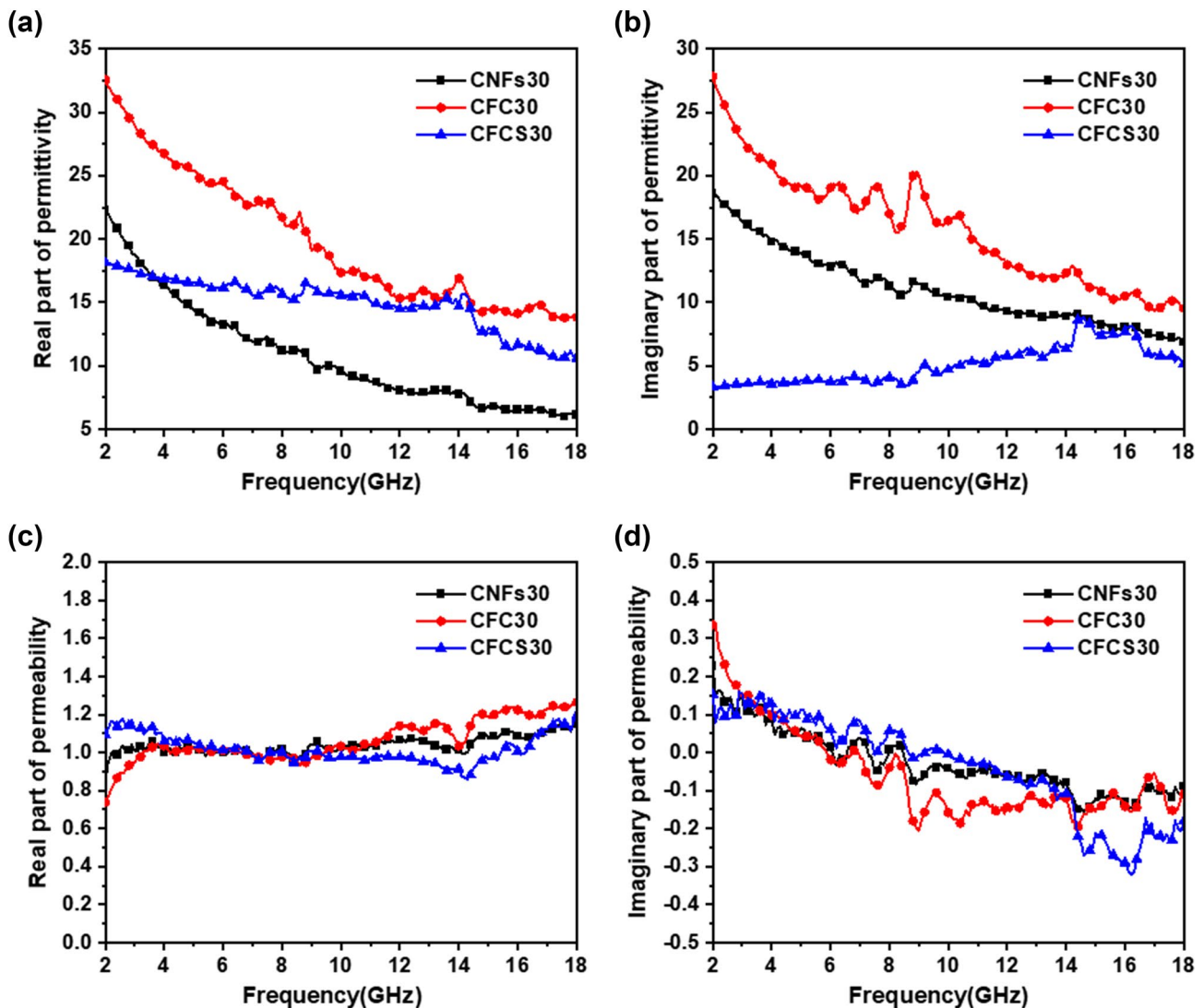


**Fig. 6** The real part of permittivity (a), the imaginary part of permittivity (b), the real part of permeability (c), and the imaginary part of permeability (d)

shown in Fig. 6, the real part of the permittivity of the three samples shows a downward trend (Fig. 6a), which is due to the lagging of the dipole polarization response relative to the variation of the electric field at high frequency increases. It is a typical dispersion behavior and often occurs in carbon materials [33, 34]. With the addition of Co-Fe nanoparticles, the real part and imaginary part of permittivity increase apparently, but after the introduction of SiO<sub>2</sub>, the real part of permittivity decreases, and the imaginary part is even lower than that of CNFs30 (Fig. 6a and b). It can be conjectured that Co-Fe nanoparticles as metal increase the conductivity of the material, while the insulator SiO<sub>2</sub> coating on the surface of carbon fiber decreases its conductivity to a great extent, which leads to the change of the imaginary part of permittivity. Its anti-dispersion ability has also been improved. In order to further explore the role of SiO<sub>2</sub>, Co-Fe nanoparticles in EM wave absorption, the loss mechanism is analyzed by Debye theory. The equation of this theory is as follows [35, 36]:

$$\epsilon' = \epsilon_\infty + \frac{\epsilon_s - \epsilon_\infty}{1 + \omega^2\tau^2} \tag{3}$$

$$\epsilon'' = \epsilon_p'' + \epsilon_c'' = \omega\tau \frac{\epsilon_s - \epsilon_\infty}{1 + \omega^2\tau^2} + \frac{\sigma}{\omega\epsilon_0} \tag{4}$$

where  $\epsilon_s$  and  $\epsilon_\infty$  are the permittivity of samples at electrostatic field and high frequency.  $\omega$  refers to the angular frequency.  $\tau$  represents the relaxation time related to frequency and temperature.  $\epsilon_0$  is the permittivity of free space.  $\epsilon_p''$  and  $\epsilon_c''$  mean polarization loss and conductive loss. In this equation, we obtain that  $\epsilon_c'' = \frac{\sigma}{\omega\epsilon_0}$ ; it just illustrates the problem of the change of conductivity before. From Fig. 6a and b, it can be seen that the imaginary part of permittivity of CNFs30 and CFC30 decreases with the increase of frequency. Through Eqs. (3) and (4), it can be determined that the dielectric loss of these two samples is mainly conductive loss, while for CFCS30, the imaginary part of permittivity increases with the increase of frequency, which shows that polarization loss is the main loss mode [37]. Then, combine the above two equations to get the following equation:

$$\left(\epsilon' - \frac{\epsilon_s + \epsilon_\infty}{2}\right)^2 + \left(\epsilon'' - \frac{\sigma}{\omega\epsilon_0}\right)^2 = \left(\frac{\epsilon_s - \epsilon_\infty}{2}\right)^2 \tag{5}$$

From the above equation, we can detect that the drawing should be a semicircle, which is called a Cole–Cole semicircle. Each semicircle represents a Debye relaxation process. Figure 7a–c shows the Cole–Cole diagram of three samples. For CNFs30, because of its high degree of graphitization (Fig. 2b can prove it), few defects, and single composition,

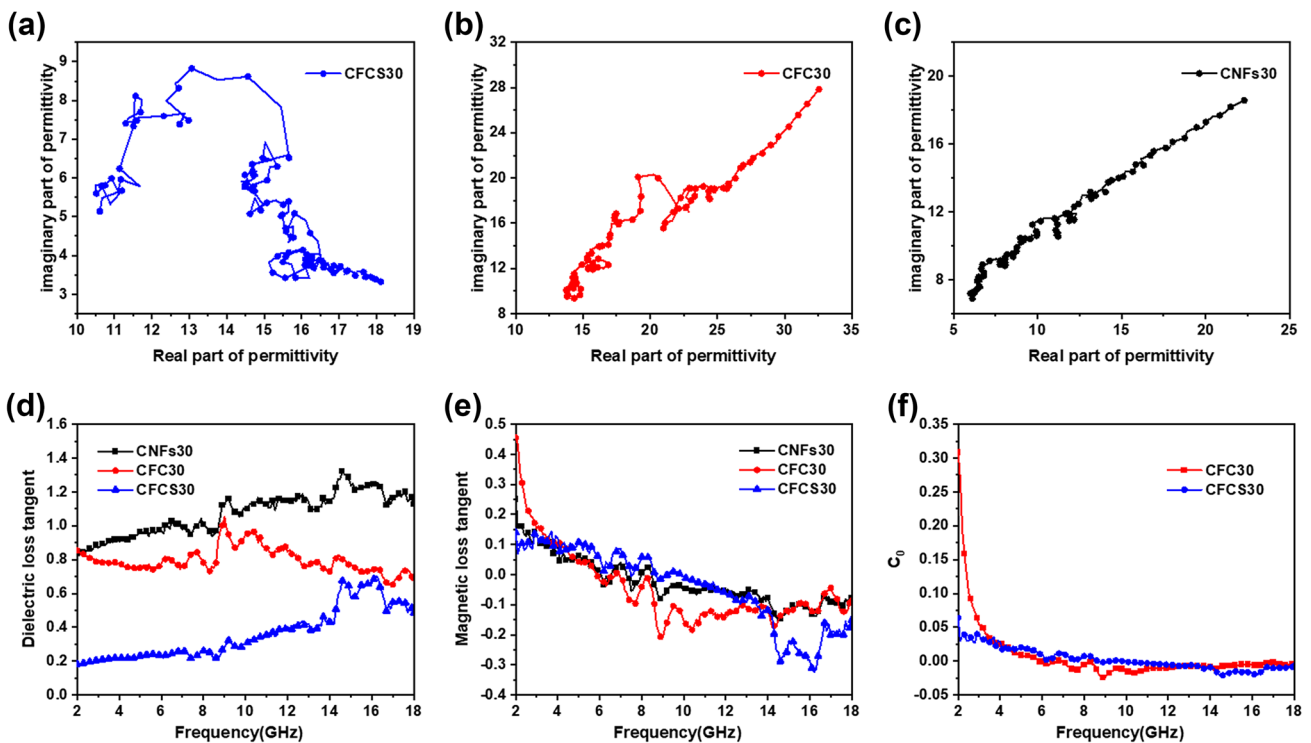


**Fig. 7** Cole–Cole diagram of CFCS30 (a), CFC30 (b), and CNFs30 (c), dielectric loss tangent (d), magnetic loss tangent (e) of CNFs30, CFC30, and CFCS30, and C<sub>0</sub> curves (f) of CFC30 and CFCS30

there is no obvious semicircle. But with the addition of Co-Fe nanoparticles and SiO<sub>2</sub>, they form a large number of heterogeneous interfaces. Due to the transfer of charge under the excitation of electromagnetic waves, the charge distribution is not uniform, which forms the electric dipole moment; this leads to the interfacial polarization [38]. At the same time, a great quantity of defects were caused by the destruction of graphite lattice by Co-Fe nanoparticles and the low crystallization degree of SiO<sub>2</sub> form polarization centers making the uneven charge distribution and resulting in dipole polarization [39].

In addition to the polarization loss, the dielectric loss also includes the conductivity loss. Because the matrix of the three samples is composed of carbon nanofibers, the carbon fibers are interlaced and stacked with each other, forming a host of conductive networks. The induced current excited by alternating electromagnetic field causes conductivity loss, which promotes the absorption of electromagnetic waves [40].

As a ferromagnetic material, Co-Fe nanoparticles not only affect the dielectric properties, but also bring magnetic loss. Generally speaking, the magnetic loss includes exchange resonance, natural resonance, domain wall resonance, eddy current loss, and hysteresis loss. However, the magnetic field produced by EM wave is low, which cannot cause irreversible wall shift and domain turning hysteresis loss in the process of dynamic magnetization. Domain wall resonance usually occurs in the MHz band [41], so these two kinds of losses are not considered. The permeability of the three samples is shown in Fig. 6c and d, and the real part of the permeability of CNFs30 is well maintained around 1. For CFC30 and CFCS30, the introduction of Co-Fe nanoparticles leads to some fluctuations in the real part of permeability. The natural resonance frequency can be calculated by the following formula [42]:

$$2\pi f_r = rH_a \quad (6)$$

$$H_a = 4|K_1|/3\mu_0M_s \quad (7)$$

where  $f_r$  is the natural resonance frequency,  $H_a$  refers to the anisotropy field,  $r$  stands for gyromagnetic ratio, and  $|K_1|$  is the anisotropy coefficient. Co-Fe nanoparticles have large surface anisotropy due to the small size effect, and the natural resonance frequency shifts to a higher frequency with the enhancement of the surface anisotropy field; that is to say, the resonance peaks at 6 GHz and 7 GHz (Fig. 6d) are caused by natural resonance. In addition, the resonance peak in the higher frequency band may be caused by exchange resonance [43]. In addition to natural resonance and exchange resonance, eddy current loss may also be a mechanism of material attenuation to EM waves, and its influencing factors include material thickness  $d$  and electrical conductivity

$\sigma$ . The specific expression formula is as follows [44]:  $\mu''(\mu')^{-2}f^{-1} = 2\pi\mu_0d\sigma$ , where  $\mu_0$  is vacuum permeability. If there is eddy current loss in the material, the value of  $\mu''(\mu')^{-2}f^{-1}$  should remain constant with the increase of frequency, and the magnitude is 0. It can be seen from Fig. 7d the curves of the two samples in 2–9 GHz and 14–18 GHz, which indicates that the eddy current loss is not the main mechanism of magnetic loss. At the same time, it shows that the imaginary part of the permeability of the sample is negative at some frequencies, although the imaginary part of the negative permeability can be reasonably explained by the implicit Fabry-Pérot resonance [45], but in fact it may be due to the excessive thickness of the sample, which is not the intrinsic characteristic of the material, or it may be caused by the induced current of the three-dimensional conductive network of the sample producing a new magnetic field under the alternating electromagnetic field. But the magnetic loss of the absorber is weak and this part of magnetic energy radiation cannot be offset, as a result, the imaginary part of negative permeability is produced [46].

For sake of knowing which of the dielectric loss and magnetic loss plays a dominant role in the EM wave absorption, the tangent of the dielectric loss angle and the magnetic loss angle are calculated. As shown in Fig. 7e and f, the tangent of the dielectric loss angle of the three samples is larger than that of the magnetic loss angle. This manifests that the dielectric loss is the main loss mode. At the same time, it can also be found that although CFCS30 has the best absorbing performance, both the tangent of dielectric loss angle and the tangent of magnetic loss angle are less than that of CFC30. To ensure the accuracy of the results, the attenuation constant  $\alpha$  of samples is calculated. The attenuation constant  $\alpha$  is a crucial standard to evaluate the attenuation ability of the material to microwave and a vital factor affecting microwave absorption. The calculation formula is as follows [47]:

$$\alpha = \frac{\sqrt{2}\pi f}{c} \times \sqrt{(\epsilon''\mu'' - \epsilon'\mu') + \sqrt{(\epsilon''\mu'' - \epsilon'\mu')^2 + (\epsilon''\mu' + \epsilon'\mu'')^2}} \quad (8)$$

where  $f$  is the frequency and  $c$  represents the velocity of light in vacuum. As shown in Fig. 8a, the attenuation constants of the three samples all increase with the increase of frequency, indicating that the sample has better EM wave attenuation ability at high frequency. At the same time, corresponding to the previous loss angle tangent, CFCS30 also does not have the highest attenuation constant, but the CFC30 with poor absorbing performance has the largest loss angle tangent and attenuation constant.

The answer to this question can be obtained by analyzing another key factor affecting EM wave absorption. Whether the electromagnetic wave can be absorbed depends on two factors, one is the attenuation constant discussed above, which represents the ability of the material to convert EM



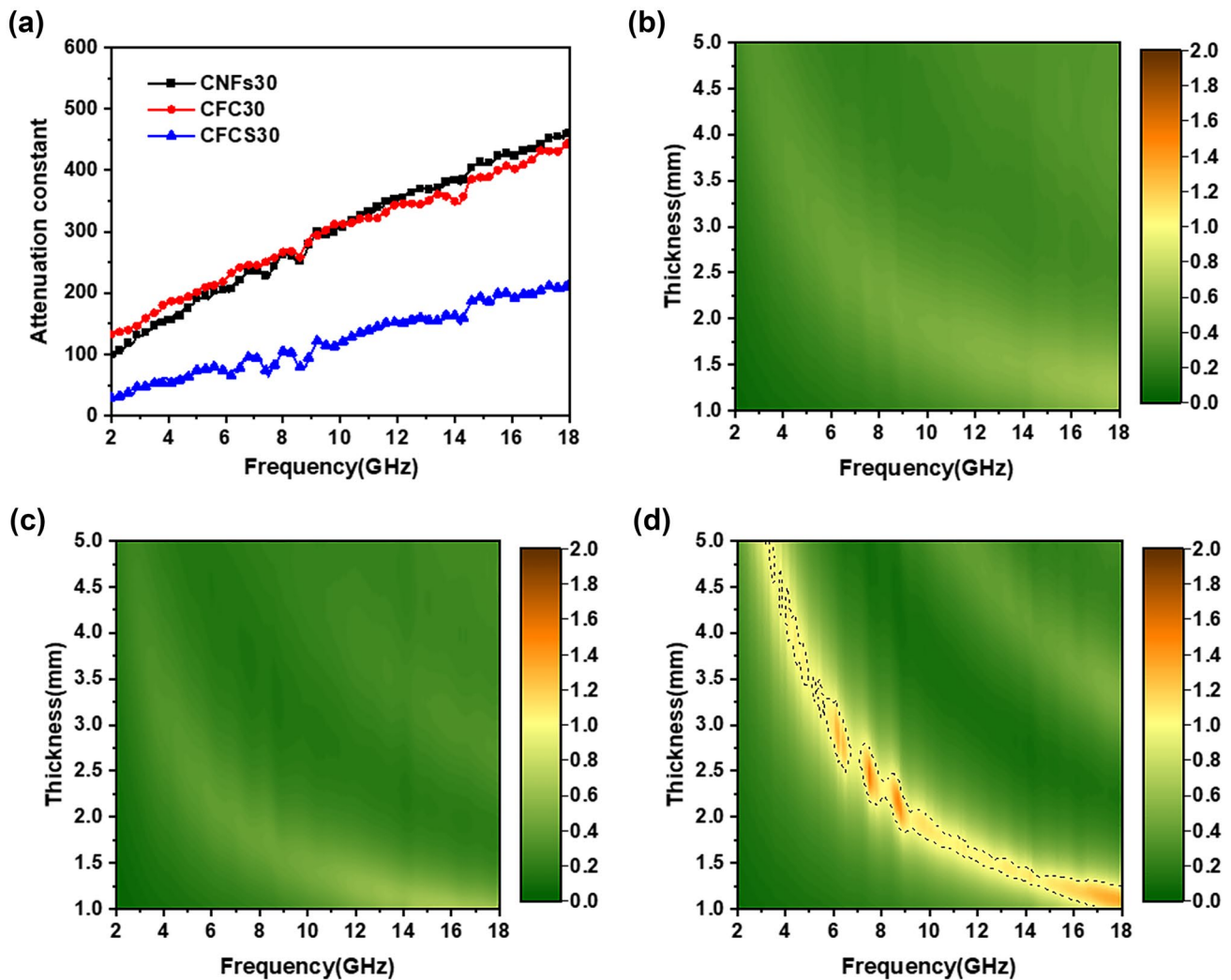


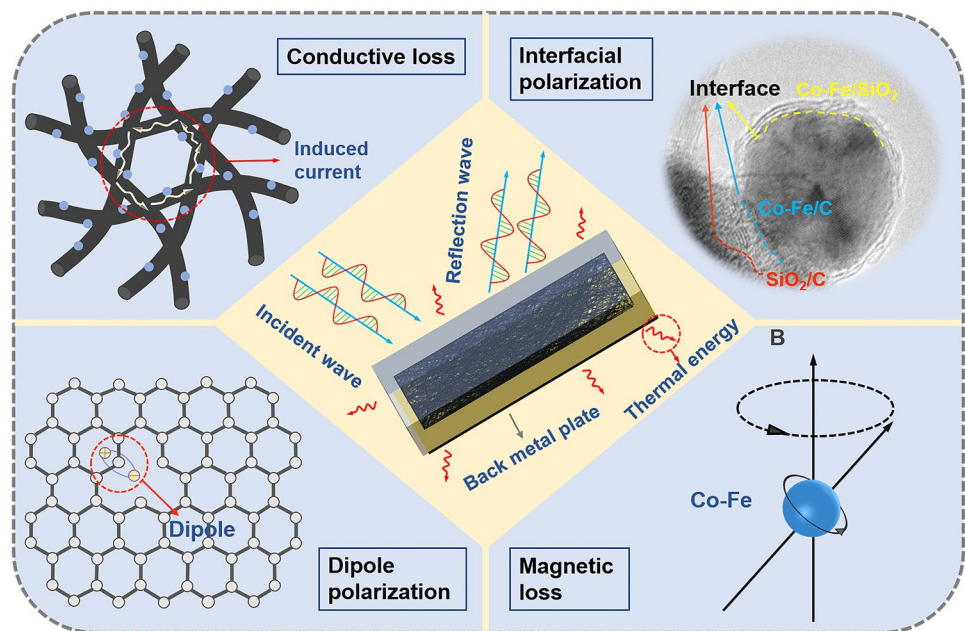
**Fig. 8** Attenuation constant (a) of CNFs30, CFC30, and CFCS30, and images of  $|Z_{in}/Z_0|$  values for CNFs30 (a), CFC30 (b), and CFCS30 (c)

wave energy into thermal energy, and the other one is impedance matching, which determines whether the electromagnetic wave can be successfully incident into the material without being reflected. The ideal impedance matching condition is that the impedance on both sides of the interface of the absorber is equal, that is  $|Z_{in}/Z_0| = 1$ . The closer the ratio is to 1, the better the impedance matching will be. The impedance matching is projected with the variation of thickness and frequency, as shown in Fig. 8b–d; for CNFs30, owing to its high degree of graphitization, it has high conductive loss, which leads to excessive imaginary part of permittivity and impedance mismatch. The introduction of Co-Fe nanoparticles makes it have more dielectric loss and magnetic loss, but it does not solve the problem of balance between permittivity and permeability. For CFC30, although  $\text{SiO}_2$  coated on carbon fiber reduces the conductivity and weakens the conductivity loss, the imaginary part of its lower permittivity is beneficial to the incidence of

electromagnetic wave and plays a critical part in improving impedance matching. It proclaims that near the range of dotted lines, the ratio of impedance matching is close to 1, and microwave can incident the material more and thoroughly brings the attenuation loss of carbon conductive network and Co-Fe nanoparticles into play.

According to the result discussed above, the main wave-absorbing mechanisms of carbon/ $\text{SiO}_2$  core-sheath nanofibers with Co-Fe nanoparticles embedded in are revealed in Fig. 9. First, the three-dimensional conductive network formed by carbon fibers contributes to the formation of induced current, and Co-Fe nanoparticles loaded on the surface of fibers improve the conductivity of the fibers and enhance the conductivity loss. Then, masses of heterogeneous interfaces are produced between carbon,  $\text{SiO}_2$ , and Co-Fe nanoparticles, and the formation of these interfaces results in the transfer of space charge, which gives rise to interfacial polarization. Furthermore, Co-Fe nanoparticles

**Fig. 9** Schematic diagram of wave-absorbing mechanism for CFC



have a certain destructive effect on graphite lattice, and the defects caused by lattice damage can be used as polarization centers to cause dipole polarization. The above three loss modes, as dielectric loss, play a leading role in microwave attenuation. Finally, Co-Fe nanoparticles can produce magnetic loss due to their own ferromagnetism, which further promotes the attenuation of microwaves.

## 4 Conclusion

In conclusion, carbon/SiO<sub>2</sub> core-sheath nanofibers with Co-Fe nanoparticles embedded in were successfully prepared by electrospinning and carbonization process, and their wave-absorbing properties were tested. It is found that Co-Fe nanoparticles can significantly reduce the matching thickness of materials and bring magnetic loss. The defects arising from the destruction of graphite lattice affected by Co-Fe nanoparticles lead to dipole polarization. The introduction of SiO<sub>2</sub> can not only improve the impedance matching of the materials, but also produce interfacial polarization caused by plenty of heterogeneous interfaces which enhance the dielectric loss ability together with dipole polarization. The conductive loss caused by the formation of conductive network of carbon nanofibers is also essential for EM wave attenuation. The wave-absorbing properties of this material are optimized under the synergistic action of three different components. The maximum RL is −59.6 dB, the maximum effective absorption bandwidth is 4.6 GHz (12.8–17.4 GHz), and the matching thickness is 1.43 mm. The results show that Co-Fe/C nanofiber coated with SiO<sub>2</sub> is a kind of lightweight

wave-absorbing material with excellent properties, which can be used as an important reference for the design and synthesis of materials based on carbon nanofibers.

**Acknowledgements** The authors thank Mr. Rui Tian, Mr. Wenjin Zhang, and Ms. Guojing Zhao for constructive discussions.

**Funding** The study was financially supported by the National Natural Science Foundation of China (Grant numbers 51601105, 51771104, and 51971119), Young Elite Scientists Sponsorship Program by CAST (Grant number 2017QNRC001), Natural Science Outstanding Youth Fund of Shandong Province (Grant number ZR2020YQ32), and China Postdoctoral Science Foundation (Grant number 2018T110687).

## Declarations

**Conflict of interest** The authors declare no competing interests.

## References

- Zhou X, Wang B, Jia Z, Zhang X, Liu X, Wang K, Xu B, Wu G (2021) Dielectric behavior of Fe<sub>3</sub>N@C composites with green synthesis and their remarkable electromagnetic wave absorption performance. *J Colloid Interface Sci* 582:515–525. <https://doi.org/10.1016/j.jcis.2020.08.087>
- Xie P, Liu Y, Feng M, Niu M, Liu C, Wu N, Sui K, Patil RR, Pan D, Guo Z, Fan R (2021) Hierarchically porous Co/C nanocomposites for ultralight high-performance microwave absorption. *Advanced Composites and Hybrid Materials* 4:173–185. <https://doi.org/10.1007/s42114-020-00202-z>
- Du H, Zhang Z, Tian R, Zhang W, Zhang J, Liu X, Sun K, Fan R (2020) Research progress in broadband absorber based on artificial electromagnetic medium. *J Mater Eng* 48:23–33. <https://doi.org/10.11868/j.issn.1001-4381.2019.001015>
- Wu N, Du W, Hu Q, Vupputuri S, Jiang Q (2020) Recent development in fabrication of Co nanostructures and their carbon

- nanocomposites for electromagnetic wave absorption. *Engineered Science* 13:11–23. <https://doi.org/10.30919/es8d1149>
5. Wang L, Song P, Lin C, Kong J, Gu J (2020) 3D shapeable, superior electrically conductive cellulose nanofibers/Ti<sub>3</sub>C<sub>2</sub>T<sub>x</sub> MXene aerogels/epoxy nanocomposites for promising EMI shielding. *Research (Wash D C)* 2020:4093732. <https://doi.org/10.34133/2020/4093732>
  6. Asmatulu R, Bollavaram PK, Patlolla VR, Alarifi IM, Khan WS (2020) Investigating the effects of metallic submicron and nanofilms on fiber-reinforced composites for lightning strike protection and EMI shielding. *Advanced Composites and Hybrid Materials* 3:66–83. <https://doi.org/10.1007/s42114-020-00135-7>
  7. Wang Z, Li X, Wang L, Li Y, Qin J, Xie P, Qu Y, Sun K, Fan R (2020) Flexible multi-walled carbon nanotubes/polydimethylsiloxane membranous composites toward high-permittivity performance. *Advanced Composites and Hybrid Materials* 3:1–7. <https://doi.org/10.1007/s42114-020-00144-6>
  8. Shu R, Zhang J, Guo C, Wu Y, Wan Z, Shi J, Liu Y, Zheng M (2020) Facile synthesis of nitrogen-doped reduced graphene oxide/nickel-zinc ferrite composites as high-performance microwave absorbers in the X-band. *Chem Eng J* 384:123266. <https://doi.org/10.1016/j.cej.2019.123266>
  9. Lv H, Li Y, Jia Z, Wang L, Guo X, Zhao B, Zhang R (2020) Exceptionally porous three-dimensional architectural nanostructure derived from CNTs/graphene aerogel towards the ultra-wideband EM absorption. *Compos B Eng* 196:108122. <https://doi.org/10.1016/j.compositesb.2020.108122>
  10. Fu X, Shi L, Cui T (2020) Research progress in terahertz metamaterials and their applications in imaging. *J Mater Eng* 48:12–22. <https://doi.org/10.1007/s42114-021-00307-z>
  11. Huang Y, Ji J, Chen Y, Li X, He J, Cheng X, He S, Liu Y, Liu J (2019) Broadband microwave absorption of Fe<sub>3</sub>O<sub>4</sub>/BaTiO<sub>3</sub> composites enhanced by interfacial polarization and impedance matching. *Compos B Eng* 163:598–605. <https://doi.org/10.1016/j.compositesb.2019.01.008>
  12. Liu X, Ren Z, Chen L, Li G, Wang Q, Zhou J (2020) Infrared stealth metamaterials. *J Mater Eng* 48:1–11. <https://doi.org/10.11868/j.issn.1001-4381.2019.001019>
  13. Wang R, Li S, Hu P, Chen S, Wang J (2021) Densification behavior and microstructure evolution of Mo nanocrystals by microwave sintering. *ES Materials & Manufacturing* 13:97–105. <https://doi.org/10.30919/esmm5f433>
  14. Liu P, Zhang Y, Yan J, Huang Y, Xia L, Guang Z (2019) Synthesis of lightweight N-doped graphene foams with open reticular structure for high-efficiency electromagnetic wave absorption. *Chem Eng J* 368:285–298. <https://doi.org/10.1016/j.cej.2019.02.193>
  15. Guo H, Zhang J, Wang Q, Bi K (2020) Ferromagnetic/ferroelectric composites and microwave properties of its metamaterial structure. *J Mater Eng* 48:43–49. <https://doi.org/10.11868/j.issn.1001-4381.2019.000980>
  16. Wu H, Wu G, Ren Y, Yang L, Wang L, Li X (2015) Co<sup>2+</sup>/Co<sup>3+</sup> ratio dependence of electromagnetic wave absorption in hierarchical NiCo<sub>2</sub>O<sub>4</sub>-CoNiO<sub>2</sub> hybrids. *J Mater Chem C* 3:7677–7690. <https://doi.org/10.1039/c5tc01716e>
  17. Liu P, Gao S, Wang Y, Huang Y, He W, Huang W, Luo J (2020) Carbon nanocages with N-doped carbon inner shell and Co/N-doped carbon outer shell as electromagnetic wave absorption materials. *Chem Eng J* 381:122653. <https://doi.org/10.1016/j.cej.2019.122653>
  18. Zhao B, Liang L, Bai Z, Guo X, Zhang R, Jiang Q, Guo Z (2021) Poly(vinylidene fluoride)/Cu@Ni anchored reduced-graphene oxide composite films with folding movement to boost microwave absorption properties. *ES Energy & Environment* <https://doi.org/10.30919/esee8c488>
  19. Huo Y, Zhao K, Xu Z, Tang Y (2020) Electrospinning synthesis of SiC/carbon hybrid nanofibers with satisfactory electromagnetic wave absorption performance. *J Alloy Compd* 815:152458. <https://doi.org/10.1016/j.jallcom.2019.152458>
  20. Zhang D, Sun J, Lee LJ, Castro JM (2020) Overview of ultrasonic assisted manufacturing multifunctional carbon nanotube nanopaper based polymer nanocomposites. *Engineered Science* 10:35–50. <https://doi.org/10.30919/es5e1002>
  21. Lu X, Zhu D, Li X, Li M, Chen Q, Qing Y (2021) Gelatin-derived N-doped hybrid carbon nanospheres with an adjustable porous structure for enhanced electromagnetic wave absorption. *Advanced Composites and Hybrid Materials*. <https://doi.org/10.1007/s42114-021-00258-5>
  22. Liu C, Fang Q, Wang D, Yan C, Liu F, Wang N, Guo Z, Jiang Q (2019) Carbon and boron nitride nanotubes: structure, property and fabrication. *ES Materials & Manufacturing* 3:2–15. <https://doi.org/10.30919/esmm5f199>
  23. Yu B, Li X, An J, Jiang Z, Yang J (2018) Interfacial and glass transition properties of surface-treated carbon fiber reinforced polymer composites under hygrothermal conditions. *Engineered Science* 2:67–73. <https://doi.org/10.30919/es8d628>
  24. Zhang W, Zhang Z, Jiang Y, Hou C, Fu X, Du H, Tian R, Zhao G, Wei S, Fan R (2020) Porous Fe@Fe<sub>3</sub>O<sub>4</sub>-C nanocomposite using polyvinyl alcohol sponge as template for microwave absorption. *J Electron Mater* 49:6394–6402. <https://doi.org/10.1007/s11664-020-08443-w>
  25. Lu Y, Wang Y, Li H, Lin Y, Jiang Z, Xie Z, Kuang Q, Zheng L (2015) MOF-derived porous Co/C nanocomposites with excellent electromagnetic wave absorption properties. *ACS Appl Mater Interfaces* 7:13604–13611. <https://doi.org/10.1021/acsami.5b03177>
  26. Xiang J, Li J, Zhang X, Ye Q, Xu J, Shen X (2014) Magnetic carbon nanofibers containing uniformly dispersed Fe/Co/Ni nanoparticles as stable and high-performance electromagnetic wave absorbers. *J Mater Chem A* 2:16905–16914. <https://doi.org/10.1039/c4ta03732d>
  27. Wang W, Zhou J, Zhang S, Song J, Duan H, Zhou M, Gong C, Bao Z, Lu B, Li X, Lan W, Xie E (2010) A novel method to fabricate silica nanotubes based on phase separation effect. *J Mater Chem* 20:9068–9072. <https://doi.org/10.1039/c0jm02120b>
  28. Li D, Liao H, Kikuchi H, Liu T (2017) Microporous Co@C nanoparticles prepared by dealloying CoAl@C precursors: achieving strong wideband microwave absorption via controlling carbon shell thickness. *ACS Appl Mater Interfaces* 9:44704–44714. <https://doi.org/10.1021/acsami.7b13538>
  29. Song Q, Ye F, Yin X, Li W, Li H, Liu Y, Li K, Xie K, Li X, Fu Q, Cheng L, Zhang L, Wei B (2017) Carbon nanotube-multilayered graphene edge plane core-shell hybrid foams for ultrahigh-performance electromagnetic-interference shielding. *Adv Mater* 29:1701583. <https://doi.org/10.1002/adma.201701583>
  30. Lyu L, Liu J, Liu H, Liu C, Lu Y, Sun K, Fan R, Wang N, Lu N, Guo Z, Wujcik EK (2018) An overview of electrically conductive polymer nanocomposites toward electromagnetic interference shielding. *Engineered Science* 2:26–42. <https://doi.org/10.30919/es8d615>
  31. Qiao J, Zhang X, Xu D, Kong L, Lv L, Yang F, Wang F, Liu W, Liu J (2020) Design and synthesis of TiO<sub>2</sub>/Co/carbon nanofibers with tunable and efficient electromagnetic absorption. *Chem Eng J* 380:122591. <https://doi.org/10.1016/j.cej.2019.122591>
  32. Shen Y, Wei Y, Li J, Li Q, Ma J, Wang P, Li B, He W, Du X (2019) Preparation of microwave absorbing Co-C nanofibers with robust superhydrophobic properties by electrospinning. *J Mater Sci: Mater Electron* 30:3365–3377. <https://doi.org/10.1007/s10854-018-00610-4>
  33. Wang H, Guo H, Dai Y, Geng D, Han Z, Li D, Yang T, Ma S, Liu W, Zhang Z (2012) Optimal electromagnetic-wave absorption by enhanced dipole polarization in Ni/C nanocapsules. *Appl Phys Lett* 101:083116. <https://doi.org/10.1063/1.4747811>

34. Wang K, Chen Y, Tian R, Li H, Zhou Y, Duan H, Liu H (2018) Porous Co-C core-shell nanocomposites derived from Co-MOF-74 with enhanced electromagnetic wave absorption performance. *ACS Appl Mater Interfaces* 10:11333–11342. <https://doi.org/10.1021/acsami.8b00965>
35. Zhao B, Deng J, Zhang R, Liang L, Fan B, Bai Z, Shao G, Park CB (2018) Recent advances on the electromagnetic wave absorption properties of Ni based materials. *Engineered Science* 3:5–40. <https://doi.org/10.30919/es8d735>
36. Jian X, Wu B, Wei Y, Dou SX, Wang X, He W, Mahmood N (2016) Facile synthesis of Fe<sub>3</sub>O<sub>4</sub>/GCs composites and their enhanced microwave absorption properties. *ACS Appl Mater Interfaces* 8:6101–6109. <https://doi.org/10.1021/acsami.6b00388>
37. Wu N, Zhao B, Liu J, Li Y, Chen Y, Chen L, Wang M, Guo Z (2021) MOF-derived porous hollow Ni/C composites with optimized impedance matching as lightweight microwave absorption materials. *Advanced Composites and Hybrid Materials*. <https://doi.org/10.1007/s42114-021-00307-z>
38. Ma J, Wang X, Cao W, Han C, Yang H, Yuan J, Cao M (2018) A facile fabrication and highly tunable microwave absorption of 3D flower-like Co<sub>3</sub>O<sub>4</sub>-rGO hybrid-architectures. *Chem Eng J* 339:487–498. <https://doi.org/10.1016/j.cej.2018.01.152>
39. Wu N, Liu C, Xu D, Liu J, Liu W, Shao Q, Guo Z (2018) Enhanced electromagnetic wave absorption of three-dimensional porous Fe<sub>3</sub>O<sub>4</sub>/C composite flowers. *ACS Sustainable Chemistry & Engineering* 6:12471–12480. <https://doi.org/10.1021/acssuschemeng.8b03097>
40. Wang F, Sun Y, Li D, Zhong B, Wu Z, Zuo S, Yan D, Zhuo R, Feng J, Yan P (2018) Microwave absorption properties of 3D cross-linked Fe/C porous nanofibers prepared by electrospinning. *Carbon* 134:264–273. <https://doi.org/10.1016/j.carbon.2018.03.081>
41. Shen Y, Wei Y, Ma J, Zhang Y, Ji B, Tang J, Zhang L, Yan P, Du X (2020) Self-cleaning functionalized FeNi/NiFe<sub>2</sub>O<sub>4</sub>/NiO/C nanofibers with enhanced microwave absorption performance. *Ceram Int* 46:13397–13406. <https://doi.org/10.1016/j.ceramint.2020.02.121>
42. Zong M, Huang Y, Zhao Y, Sun X, Qu C, Luo D, Zheng J (2013) Facile preparation, high microwave absorption and microwave absorbing mechanism of RGO-Fe<sub>3</sub>O<sub>4</sub> composites. *RSC Adv* 3:23638–23648. <https://doi.org/10.1039/c3ra43359e>
43. Aharoni A (1991) Exchange resonance modes in a ferromagnetic sphere. *J Appl Phys* 69:7762–7764. <https://doi.org/10.1063/1.347502>
44. Lv H, Zhang H, Zhao J, Ji G, Du Y (2016) Achieving excellent bandwidth absorption by a mirror growth process of magnetic porous polyhedron structures. *Nano Res* 9:1813–1822. <https://doi.org/10.1007/s12274-016-1074-1>
45. Hou Z-L, Zhang M, Kong L-B, Fang H-M, Li Z-J, Zhou H-F, Jin H-B, Cao M-S (2013) Microwave permittivity and permeability experiments in high-loss dielectrics: caution with implicit Fabry-Pérot resonance for negative imaginary permeability. *Appl Phys Lett* 103:162905. <https://doi.org/10.1063/1.4825378>
46. Li Z, Han X, Ma Y, Liu D, Wang Y, Xu P, Li C, Du Y (2018) MOFs-derived hollow Co/C microspheres with enhanced microwave absorption performance. *ACS Sustainable Chemistry & Engineering* 6:8904–8913. <https://doi.org/10.1021/acssuschemeng.8b01270>
47. Jiang Y, Fu X, Tian R, Zhang W, Du H, Fu C, Zhang Z, Xie P, Xin J, Fan R (2020) Nitrogen-doped carbon nanofibers with sulfur heteroatoms for improving microwave absorption. *J Mater Sci* 55:5832–5842. <https://doi.org/10.1007/s10853-020-04430-y>

**Publisher's Note** Springer Nature remains neutral with regard to jurisdictional claims in published maps and institutional affiliations.